Published in final edited form as:
J Colloid Interface Sci. 2014 September 15; 430: 257–264. doi:10.1016/j.jcis.2014.04.053.

ZnO and cobalt phthalocyanine hybridized graphene: efficient photocatalysts for degradation of rhodamine B

Gururaj M. Neelgund[a], **Aderemi Oki**[a,*], and **Zhiping Luo**[b]

[a]Department of Chemistry, Prairie View A&M University, Prairie View, TX 77446, USA

[b]Microscopy and Imaging Center and Materials Science and Engineering Program, Texas A&M University, College Station, TX 77843, USA

Abstract

A novel method has been developed to synthesize graphene-ZnO composite as a highly efficient catalyst by reduction of graphite oxide and *in-situ* deposition of ZnO nanoparticles by chemical reduction reaction. The graphene-ZnO catalyst is capable of complete degradation of rhodamine B under exposure to natural sunlight. Further, the catalytic efficiency of graphene-ZnO catalyst was enhanced by sensitizing with cobalt phthalocyanine. The formation of graphene-ZnO pcatalyst and its further sensitization with cobalt phthalocyanine was characterized using UV-vis, ATR-IR and Raman spectroscopy, powder XRD and thermogravimetric analysis. The morphology of both graphene-ZnO and graphene-ZnO-CoPC catalysts was analyzed using scanning and transmission electron microscopes.

Keywords

Graphene; Zinc oxide; Photocatalyst; Cobalt phthalocyanine; Rhodamine B

1. Introduction

Allotropes of carbon of different dimensionalities, such as one dimensional carbon nanotubes (CNTs) and two dimensional graphene, have opened up new opportunities to design and develop nanocomposites with unique properties for variety of applications [1–7]. In comparison with CNTs, graphene possesses similar physical properties but larger surface area, which can be considered as an unrolled CNT [8,9]. In addition, the production cost of graphene sheets in large quantities is much lower than that of CNTs [10,11]. Therefore, graphene as a low cost alternative to CNTs in composites is highly expected [12]. Monolayer graphene, possessing a unique two dimensional layer structure of sp^2-hybridized carbon atoms, exhibits novel electronic property as a zero-band gap semiconductor and is highly electronically conductive for storing and transporting electrons [13–15]. One possible

*Corresponding author: Fax: +1-936-261-3117, aroki@pvamu.edu (A. Oki).

way to utilize the unique properties of graphene would be its incorporation in a composition. In this regard, graphene-semiconductor composites have been attracted much attention and could provide new ways to design graphene based composites for catalytic and photocatalytic reactions [16]. This functionalization can be attributed to the electron transfer from the conduction band of semiconductor to graphene [10,17]. In the meantime, such an modification of graphene with metal oxide particles may also prevent the restack and agglomeration of graphene sheets during the reduction process due to van der Waals interactions between them [18,19]. Moreover, Due to excellent electron accepting property of graphene, [20,21] it can be expected that presence of graphene in the composites will enhance catalytic performance of the semiconductor [22].

Zinc oxide is an important member in the II–VI group semiconductors, which has a wide band gap of 3.20 eV and a large binding energy of 60 meV [23]. It has profound applications in optics, optoelectronics, sensors, and actuators due to its semiconducting, piezoelectric, and pyroelectric properties [24]. The potential use of ZnO in photocatalysis has particularly aroused great interest, as there have been several examples of ZnO displaying superior photocatalytic decomposition of organics [25,26]. Recent investigations demonstrated that photocatalytic efficiency of ZnO enhances by the combination of graphene [15,27,28]. Li and Cao reported the incorporation of graphene with ZnO to form ZnO@graphene composite via a chemical deposition route and evaluated its photocatalytic activity in terms of degradation of rhodamine B (RhB) under UV and visible light irradiation [15]. Xu et al. prepared ZnO/graphene composite and estimated its photocatalytic activity through degradation of methylene blue [27]. Yang et al. fabricate a hybrid structure by anchoring ZnO nanoparticles on functionalized graphene sheets using poly(vinyl pyrrolidone) as an intermediate and investigated its photocatalytic property by degradation of Rhodamine B [28].

In this article, we demonstrated a facile and rapid single step method for reduction of graphene oxide to graphene and *in-situ* deposition of ZnO particles over graphene nanosheets. The resulting graphene-ZnO (GR-ZnO) photocatalyst was characterized using UV–vis spectrophotometer, Fourier transform infrared spectroscopy (FTIR), Raman spectroscopy, powder X-ray diffraction (XRD), scanning electron microscopy (SEM), transmission electron microscopy (TEM), Raman spectroscopy and thermogravimetric analysis (TGA). The catalytic activity of GR-ZnO catalyst has been explored through degradation of an important dye, Rhodamine B (RhB) under exposure to natural sunlight. Further the photodegradation efficiency of GR-ZnO catalyst was enhanced by sensitizing with cobalt phthalocyanine (CoPC).

2. Experimental

2.1. Materials

All the reagents were purchased from Aldrich and used without further purification unless otherwise noted. All the aqueous solutions were prepared with ultrapure water obtained from Milli-Q Plus system (Millipore).

2.2. Preparation of GO

Graphene oxide (GO) was prepared from graphite powder according to the Hummers and Offeman method with slight modifications [29]. In a typical procedure, 1 g graphite powder (<20 μm, Aldrich) was added into 40 mL concentrated H_2SO_4 and stirred for 1 h under ice-cooling condition. Then 15 mL fuming HNO_3 was slowly added and stirred the mixture for 30 min. To this, 5 g $KMnO_4$ was gradually added with stirring and cooling. The resulting mixture was then stirred at room temperature for 12 h followed by addition of 150 mL DI water. After 30 mins of stirring, 30 mL H_2O_2 (30%) was slowly added, immediately the color of the reaction mixture was turned to bright yellow. This reaction mixture was centrifuged and washed with 1:10 HCl solution in order to remove metal ions. Then the mixture was washed with DI water until removal of acid. Thus obtained dark-yellow colored GO was dried under vacuum at 40 °C for 12 h. The drying process of GO was carried out at lower temperature in order to avoid deoxygenation.

2.3. Preparation of GR-ZnO catalyst

GO (40 mg) was dispersed in DI water (25 mL) by sonication for 5 min and a solution of 0.01 mol L^{-1} of $ZnCl_2$ in 20 mL DI water was added. The resulting suspension was stirred for 15 mins followed by addition of hydrazine hydrate (2 mL). Then the reaction was allowed to proceed at room temperature for 1 h. Thus produced GR-ZnO composite was separated by centrifugation, successively washed with DI water and dried under vaccum.

2.4. Sensitization of GR-ZnO catalyst with CoPC

GR-ZnO composite (20 mg) was dispersed in DI water (25 mL), to this a solution of CoPC (2 mg) in 5 mL dimethyl sulfoxide was added. Then the mixture was stirred in room temperature for 2 hrs. The resulting GR-ZnO-CoPC catalyst was separated by centrifugation, washed with DI water and dried under vaccum.

The overall procedure of preparation of GR-ZnO and GR-ZnO-CoPC catalysts has been schematically depicted in Scheme I.

2.5. Photocatalytic activity

The photocatalytic activity of GR-ZnO and GR-ZnO-CoPC catalysts was evaluated by degradation efficiency of RhB under exposure to natural sunlight. The average intensity of sunlight was measured using Light Meter (LX1010B), which was found to be 700–800 W/m^2. The photocatalytic experiment was performed in natural atmosphere, without any external source of aeration. In each experiment, 10 mg of catalyst was suspended in 100 mL aqueous solution of RhB (10 mg L^{-1}). This suspension was magnetically stirred in dark for 30 mins in order to establish adsorption/desorption equilibrium of RhB molecules on the surface of catalysts. Then it was transferred to a double walled quartz photocatalytic reactor with water circulation facility to maintain the reaction mixture at room temperature. The suspension was then exposed to natural sunlight under constant stirring. At a given interval of time, 5 mL of suspension was taken out, centrifuged and the concentration of RhB was analyzed by measuring its absorbance using UV-vis spectrophotometer. The normalized concentration of RhB after exposing to sunlight was calculated as C/C_0, where C_0 is the initial concentration of RhB and C is the concentration of RhB measured after exposure at a

particular interval of time All the experiments were performed under direct sunlight during June between 1 pm to 4 pm.

2.6. Characterization

ATR-IR spectra were recorded using Smiths ChemID diamond attenuated total reflection (DATR) spectrometer and TGA were performed with a Perkin Elmer Diamond TG/DTA instrument at a heating rate of 10 °C/min. Powder XRD patterns were recorded on Scintag X-ray diffractometer (PAD X), equipped with Cu Kα photon source (45 kV, 40 mA) at scanning rate of 3°/min. SEM measurements were carried out on a JEOL JXA-8900 microscope and TEM images were obtained with a JEOL 2010 microscope. Raman spectra were recorded with Renishaw R-3000QE system in the backscattering configuration using an Argon ion laser with wavelength 785 nm.

3. Results and Discussion

Fig. 1 shows the FESEM images of GO and GR-ZnO catalyst. The effective exfoliation of GO nanosheets and their porous structure generated by opening of planer carbon networks wedged at the edge surface of crystallite by oxidation process can be seen in Figs. 1a and b. Also, it is observable that GO sheets have two-dimensional structure and their surface is wrinkled. In GR-ZnO catalyst, the GR nanosheets are densely populated with rice grain morphological ZnO particles and these particles are well adhered onto GR nanosheets (Figs. 1c–f). The size of ZnO particles was found to be several micrometers and their surface was rough in nature. In Figs. 1d and e, the corrugated and scrolled GR nanosheets, resemble crumpled silk veil waves. The sensitization of GR-ZnO catalyst with CoPC did not affect much on its surface and structure (Figs. 2a–c).

Fig. 3 shows the UV-vis absorption spectra of GO, GR-ZnO catalyst, ZnO and GR-ZnO-CoPC catalyst. The spectrum of GO (Fig 3a) displayed an absorption band at 229 nm and a shoulder around 300 nm, these could be assigned to $\pi \rightarrow \pi^*$ transitions of aromatic C-C bonds and $n \rightarrow \pi^*$ transitions of C=O bonds [30–32]. The GR-ZnO catalyst (Fig 3b) demonstrated the absorption band corresponding to $\pi \rightarrow \pi^*$ transitions red shifted to 271 nm, which is consistent with the absorption of aqueous stable graphene sheets, suggesting that the electronic conjugation within the graphene sheets is restored after the reduction [33]. In addition, the characteristic absorption band corresponding to ZnO was appeared at 374 nm for GR-ZnO catalyst, which is consistent with the value (376 nm) measured for ZnO (Fig 3c). The spectrum of GR-ZnO-CoPC catalyst (Fig 3d) displayed both the characteristic absorption bands corresponding to graphene and ZnO at 276 and 373 nm, respectively. Whereas, the absorption band due to CoPC was not displayed for GR-ZnO-CoPC catalyst, it might be due to low concentration of CoPC.

ATR-IR spectra of GO, GR-ZnO catalyst and GR-ZnO-CoPC catalyst are shown in Fig. 4. The spectrum of GO (Fig. 4a) displayed the bands at 3395, 1719, 1619, 1377 and 1039 cm^{-1} are ascribed to -OH stretching, C=O stretching vibrations in carboxylic acid, skeletal vibrations of unoxidized graphitic domains, O-H deformations of the C-OH groups and stretching vibrations of alkoxy C-O groups situated at the edges of GO sheets, respectively. However, the absorption bands related to oxygen containing functional groups are vanished

in the spectrum of GR-ZnO catalyst (Fig. 4b), in addition a new band owing to skeletal vibration of the graphene sheets was appeared at 1491 cm^{-1}. These conformational changes appeared in the spectrum of GR-ZnO catalyst demonstrate the successful reduction of GO sheets to GR nanosheets in presence of hydrazine hydrate. In case of GR-ZnO-CoPC catalyst, the spectrum exhibited characteristic bands related to CoPC (Figure 4c). The main peak observed at 729 cm^{-1} was assigned to non-planar deformation vibrations of C-H bonds of benzene ring and the band at 1085 cm^{-1} was owing to C-N stretching vibrations. Among them the C-H in-plane bending vibration was displayed at 1118 cm^{-1}. The bands at 753 and 777 cm^{-1} also corresponds to non-planar vibrations (out-of-plane bending) of the C-H bonds. The band at 1422 cm^{-1} was assigned to C–C benzene ring skeletal stretching vibrations. The weak band at 909 cm^{-1} was due to metal ligand (M-N) vibration. The remaining bands at 1287 and 1329 cm^{-1} were well agreed with the frequencies reported for metal phthalocyanines [34].

Figs. 5a–d shows the XRD patterns recorded for graphite, GO, GR-ZnO catalyst and GR-ZnO-CoPC catalyst, respectively. Graphite (Fig. 5a) displayed a high intense peak at 26.4° owing to (0 0 2) plane of graphite, corresponding to interlayer d-spacing of 0.337 nm. After oxidation, the characteristic peak in GO (Fig. 5b) was appeared at 9.86°, which indicates the complete oxidation of graphite to GO and disruption of ordering of graphene layers in graphite. The interlayer d-spacing in GO was increased from to 0.337 to 0.896 nm, which is ascribed to presence of oxygen containing functional groups such as carboxyl (-COOH), hydroxyl (-OH), epoxy groups and inserted H_2O molecules. The peak corresponding to (1 0 0) plane of GR was also observed for GO at 42.6°. For GR-ZnO catalyst (Fig. 5c) the characteristic peak due to (0 0 2) plane was appeared at 26.2°, corresponding to interlayer d-spacing of 0.339 nm. This confirms the successful removal of oxygen containing functional groups and water molecules in addition to perfect exfoliation of GR sheets. The broadened peak of (0 0 2) plane appeared for GR-ZnO catalyst demonstrate the formation of smaller sized GR sheets compared to both natural graphite and GO. Moreover, GR-ZnO catalyst exhibited the additional peaks at 31.78, 34.44, 36.24, 47.56, 56.56, 62.94, 68.04 and 69.04°, these were assigned to (1 0 0), (0 0 2), (1 0 1), (1 0 2), (1 1 0), (1 0 3), (1 1 2) and (2 0 1) planes of ZnO, respectively (JCPDS file No. 36-1451). The GR-ZnO-CoPC catalyst (Fig. 5d) exhibited all the peaks analogous to GR-ZnO catalyst, in addition to peaks at 7.04, 9.26, 23.84, 33.08 and 40.43 corresponding to CoPC (JCPDS file No. 44-1994). Overall, XRD study illustrates the successful oxidation of graphite to GO, its reduction to GR nanosheets and *in-situ* deposition of ZnO, and sensitization of GR-ZnO with CoPC.

Fig. 6 compares the Raman spectra of GO and GR-ZnO catalyst. Both, GO (Fig. 6a) and GR-ZnO catalyst (Fig. 6b) displayed the distinct G-band due to E_{2g} vibrational mode of sp^2 bonded carbon around 1595 cm^{-1} (1598 cm^{-1} for GO and 1590 cm^{-1} GR-ZnO catalyst) and the d-band around 1328 cm^{-1} (1328 cm^{-1} for GO and 1327 cm^{-1} GR-ZnO catalyst) owing to the A_{1g} mode breathing vibrations of six-membered sp^2 carbon rings around. The ratio of intensity of D- to G-band (ID/IG) for GR-ZnO catalyst (1.17) was found to be higher than the ratio of GO (1.14), which indicates an increase in the number of smaller sp^2 domains in the GR-ZnO catalyst [35,36].

To further characterize the morphology of GR-ZnO and GR-ZnO-CoPC catalysts, TEM analysis was performed and the results are shown in Fig.7. It can be seen in Figs. 7a–d for GR-ZnO catalyst that the GR sheets those are larger than several micrometers are decorated with ZnO crystallites. The GR sheets are not perfectly flat but display intrinsic microscopic roughening and out of plane deformations (wrinkles). The contrast of graphene sheets is very low in the images because of the thin thickness of the sheets. The images at different magnifications show that GR-ZnO catalyst consisted of two-dimensional GR sheets and ZnO particles are well-separated from each other. Moreover, no ZnO particles were found outside the graphene sheets, which indicate the high stability of GR-ZnO composites owing to existence of strong interaction between graphene sheets and ZnO. After sensitizing the GR-ZnO catalyst with CoPC, no major difference in the morphology of GR-ZnO-CoPC catalyst (Figs. 7e–f) was observed, rather some densification was viewed due to deposition of CoPC. Fig. 7f shows a corrugated and curly graphene nanosheet, having thickness of around 10 nm. It has been reported that corrugation and scrolling are part of the intrinsic nature of graphene, which results from the fact that the 2D membrane structure becomes thermodynamically stable through bending [37].

The conversion of GO to graphene, loading of ZnO particles on graphene and the presence of CoPC in GR-ZnO-CoPC catalyst were determined by TGA. The thermograms obtained for GO, GR-ZnO catalyst and GR-ZnO-CoPC catalyst is shown in Fig. 8. The weight loss occurred below 150 °C for GO (Fig. 8a) was attributed to desorption of physisorbed water and the major weight loss observed for GO around 180 °C was ascribed to removal of oxygen-containing groups accompanied by the liberation of COx and H_2O species [38,39]. The initial weight loss observed below 100 °C for GR-ZnO (Fig. 8b) was caused by the loss of water absorbed on the surface, while the following weight loss displayed below 400 °C was attributed to the loss of the residual (or absorbed) solvent and the decomposition of residual organic functional groups on GR [40,41]. The subsequent weight loss occurred between 470 °C and 600 °C was assigned to oxidation of GR. The GR-ZnO catalyst showed an enhanced thermal stability than GO due to removal of oxygen-containing functional groups by hydrazine reduction. The weight loss around 180 °C was not observed in Fig. 8b, indicating that GO has completely reduced to graphene. The GR-ZnO-CoPC catalyst (Fig. 8c) exhibited similar thermal behavior as that of GR-ZnO catalyst, only the observed difference was in its weight loss ratio. The residual weight estimated for GR-ZnO and GR-ZnO-CoPC catalysts at 800 °C was 23% and 25%, respectively. The differences observed in the thermal behavior of GO, GR-ZnO catalyst and GR-ZnO-CoPC catalyst facilitate that their structures are different.

The catalytic activity of GR-ZnO and GR-ZnO-CoPC catalysts was evaluated by degradation of RhB under exposure to natural sunlight. The change in optical absorption of RhB in presence of GR-ZnO and GR-ZnO-CoPC catalysts at different time intervals is shown in Figs. 9(a) and (b), respectively. The decrease in the intensity of electronic absorption spectra indicates the degradation of RhB in presence of GR-ZnO and GR-ZnO-CoPC catalysts. The disappearance of characteristic absorption band of Rh B around 554 nm in Figs. 9(a) and (b) shows the complete degradation of Rh B by GR-ZnO and GR-ZnO-CoPC catalysts. Figs. 10(a) and (b) show the degradation profile of RhB in presence of CoPC, GO, GR, ZnO and GR-ZnO and GR-ZnO-CoPC catalysts at different time of

exposure to sunlight. In the absence of catalyst, the degradation of RhB was negligible even after long-time irradiation, which indicates that the self-photosensitization of RhB could be absolutely low. The RhB was completely degraded by GR-ZnO and GR-ZnO-CoPC catalysts at 140 and 150 mins of exposure, respectively. While, complete degradation of RhB did not occur in presence of CoPC, GO, GR, and ZnO at its exposure up to 140 mins. Under identical experimental conditions, the catalytic efficiency of GR-ZnO-CoPC catalyst was found to be higher than GR-ZnO catalyst. The enhancement in the photocatalytic activity of GR-ZnO compared to neat ZnO might be due to the interactions of GR nanosheets and ZnO particles. The existence of graphene nanosheets in GR-ZnO catalyst not only catalyzes the degradation of RhB but can also adsorb the RhB molecules [15]. The sensitization of GR-ZnO with CoPC further enhanced its photo-absorption ability.

It is known that the GR nanosheets behave as the electron acceptor and transporter in the GR and semiconductor composites owing to their two-dimensional π-conjugation structure [42,43]. In GR-ZnO catalyst, the photoexcited electrons can be transferred from the conduction band of ZnO particles to the conductive GR nanosheets. Hence GR nanosheets serve as an acceptor of the photoexcited electrons from ZnO particles. Those charge carriers were rapidly transferred on the two dimensional planar structure of the GR nanosheets. In this fashion, the recombination of photogenerated electrons and holes effectively suppresses and leaves more charge carriers to form reactive species, which promotes the degradation of RhB [17,44].

4. Conclusions

In summary, GR-ZnO composite, a pollutant adsorbent and photocatalyst has been successfully fabricated by in-situ reduction of GO and deposition of ZnO particles. The GR in GR-ZnO possessed great adsorptivity of RhB dye molecules and ZnO particles degraded the RhB under exposure to naturual sunlight. The excellent photocatalytic activity of GR-ZnO was attributed to large surface area of graphene nanosheets and its high adsorption capacity, and a good acceptor of electron favors the transfer of photo-generated electrons from the conduction band of ZnO to the graphene. Further, the sensitization of GR-ZnO with CoPC has improved the photoresponsivity and enhanced the photocatalytic activity. Overall, GR-ZnO and GR-ZnO-CoPC composites present a promising way for addressing environmental pollution. Also, these catalysts have good photocatalytic stability and can be reused without losing their activity for several times. Thus, the GR-ZnO and GR-ZnO-CoPC nanocomposites are efficient photocatalytic materials for degrading contaminated colored wastewater for reuse in industries.

Acknowledgments

The authors acknowledge the support from NIH-NIGMS grant #1SC3GM086245, the Welch foundation and PVAMU grant # L0002.

References

1. Huang Y, Zhao S, Liu Y, Chen J, Chen Z, Shi M, Liang H. An amplified single-walled carbon nanotube-mediated chemiluminescence turn-on sensing platform for ultrasensitive DNA detection. Chem Commun. 2012; 48:9400–9402.

2. Neelgund GM, Oki A, Luo Z. Antimicrobial activity of CdS and Ag2S quantum dots immobilized on poly(amidoamine) grafted carbon nanotubes. Colloids Surf, B. 2012; 100:215–221.
3. Wu Y, Phillips JA, Liu H, Yang R, Tan W. Carbon nanotubes protect DNA strands during cellular delivery. ACS Nano. 2008; 2:2023–2028. [PubMed: 19206447]
4. Neelgund GM, Oki A. Photocatalytic activity of CdS and Ag2S quantum dots deposited on poly(amidoamine) functionalized carbon nanotubes. Appl Catal B: Environ. 2011; 110:99–107.
5. Neelgund GM, Oki A. Pd nanoparticles deposited on poly(lactic acid) grafted carbon nanotubes: Synthesis, characterization and application in Heck C–C coupling reaction. Appl Catal A: General. 2011; 399:154–160.
6. Yu X, Kuai L, Geng B. CeO_2/rGO/Pt sandwich nanostructure: rGO-enhanced electron transmission between metal oxide and metal nanoparticles for anodic methanol oxidation of direct methanol fuel cells. Nanoscale. 2012; 4:5738–5743. [PubMed: 22893017]
7. Zheng Z, Dua Y, Fenga Q, Wanga Z, Wanga C. Facile method to prepare Pd/graphene-polyaniline nanocomposite and used as new electrode material for electrochemical sensing. J Mol Catal A: Chem. 2012; 353–354:80–86.
8. Niyogi S, Bekyarova E, Itkis ME, McWilliams JL, Hamon MA, Haddon RC. Solution properties of graphite and graphene. J Am Chem Soc. 2006; 128:7720–7721. [PubMed: 16771469]
9. Dikin DA, Stankovich S, Zimney EJ, Piner RD, Dommett GHB, Evmenenko G, Nguyen ST, Ruoff RS. Preparation and characterization of graphene oxide paper. Nature. 2007; 448:457–460. [PubMed: 17653188]
10. Stankovich S, Dikin DA, Dommett GHB, Kohlhaas KM, Zimney EJ, Stach EA, Piner RD, Nguyen ST, Ruoff RS. Graphene-based composite materials. Nature. 2006; 442:282–286. [PubMed: 16855586]
11. Xu YX, Bai H, Lu GW, Li C, Shi GQ. Flexible graphene films via the filtration of water-soluble noncovalent functionalized graphene sheets. J Am Chem Soc. 2008; 130:5856–5857. [PubMed: 18399634]
12. Lv X, Huang Y, Liu ZB, Tian JG, Wang Y, Ma YF, Liang JJ, Fu SP, Wan XJ, Chen YS. Photoconductivity of bulk-film-based graphene sheets. Small. 2009; 5:1682–1687. [PubMed: 19360726]
13. Allen MJ, Tung VC, Kaner RB. Honeycomb carbon: a review of graphene. Chem Rev. 2010; 110:132–145. [PubMed: 19610631]
14. Rao CNR, Sood AK, Subrahmanyam KS, Govindaraj A. Graphene: the new two-dimensional nanomaterial. Angew Chem, Int Ed. 2009; 48:7752–7777.
15. Li B, Cao H. ZnO@graphene composite with enhanced performance for the removal of dye from water. J Mater Chem. 2011; 21:3346–3349.
16. Das B, Choudhury B, Gomathi A, Manna AK, Pati SK, Rao CNR. Interaction of inorganic nanoparticles with graphene. Chem Phys Chem. 2011; 12:937–943. [PubMed: 21384487]
17. Zhang H, Lv X, Li Y, Wang Y, Li J. P25-graphene composite as a high performance photocatalyst. ACS Nano. 2010; 4:380–386. [PubMed: 20041631]
18. Paek SM, Yoo EJ, Honma I. Enhanced cyclic performance and lithium storage capacity of SnO_2/graphene Nanoporous electrodes with three-dimensionally delaminated flexible structure. Nano Lett. 2009; 9:72–75. [PubMed: 19090687]
19. Lu T, Pan L, Li H, Zhu G, Lv T, Liu X, Sun Z, Chen T, Chua DHC. Microwave-assisted synthesis of graphene-ZnO nanocomposite for electrochemical supercapacitors. J Alloys Compd. 2011; 509:5488–5492.
20. Manga KK, Zhou Y, Yan YL, Loh KP. Multilayer hybrid films consisting of alternating graphene and titania nanosheets with ultrafast electron transfer and photoconversion properties. Adv Funct Mater. 2009; 19:3638–3643.
21. Guo CX, Yang HB, Sheng ZM, Lu SZ, Song QL, Li CM. Layered graphene/quantum dots for photovoltaic devices. Angew Chem, Int Ed. 2010; 49:3014–3017.
22. Xiong ZG, Zhang LL, Ma JZ, Zhao XS. Photocatalytic degradation of dyes over graphene-gold nanocomposites under visible light irradiation. Chem Commun. 2010; 46:6099–6101.
23. Liu Y, Han G, Li Y, Jin M. Flower-like zinc oxide deposited on the film of graphene oxide and its photoluminescence. Mater Lett. 2011; 65:1885–1888.

24. Gao PX, Wang ZL. High-yield synthesis of single-crystal nanosprings of ZnO. Small. 2005; 1:945–949. [PubMed: 17193373]
25. Lu Y, Wang L, Wang D, Xie T, Chen L, Lin Y. A comparative study on plate- like and flower-like ZnO nanocrystals surface photovoltage property and photocatalytic activity. Mater Chem Phys. 2011; 129:281–287.
26. Sato K, Aoki M, Noyori R. A “green” route to adipic acid: direct oxidation of cyclohexenes with 30 percent hydrogen peroxide. Science. 1998; 281:1646–1647. [PubMed: 9733504]
27. Xu T, Zhang L, Cheng H, Zhu Y. Significantly enhanced photocatalytic performance of ZnO via graphene hybridization and the mechanism study. Appl Catal B: Environ. 2011; 101:382–387.
28. Yang Y, Ren L, Zhang C, Huang S, Liu T. Facile fabrication of functionalized graphene sheets (FGS)/ZnO nanocomposites with photocatalytic property. ACS Appl Mater Interfaces. 2011; 3:2779–2785. [PubMed: 21682271]
29. Hummers WS, Offeman RE. Preparation of graphitic oxide. J Am Chem Soc. 1958; 80:1339.
30. Paredes JI, Villar-Rodil S, Martinez-Alonso A, Tascon JMD. Graphene Oxide Dispersions in Organic Solvents. Langmuir. 2008; 24:10560–10564. [PubMed: 18759411]
31. Li L, Liu K, Yang G, Wang C, Zhang J, Zhu J. Fabrication of graphene-quantum dots composites for sensitive electrogenerated chemiluminescence immunosensing. Adv Funct Mater. 2011; 21:869–878.
32. Yang Y, Liu T. Fabrication and characterization of graphene oxide/zinc oxide nanorods hybrid. Appl Surf Sci. 2011; 257:8950–8954.
33. Li D, Mueller MB, Gilje S, Kaner RB, Wallace GG. Processable aqueous dispersions of graphene nanosheets. Nat Nanotechnol. 2008; 3:101–105. [PubMed: 18654470]
34. Salinas-Guzman RR, Guzman-Mar JL, Hinojosa-Reyes L, Peralta-Hernandez JM, Hernandez-Ramirez A. Enhancement of cyanide photocatalytic degradation using sol-gel ZnO sensitized with cobalt phthalocyanine. J Sol-Gel Sci Technol. 2010; 54:1–7.
35. Gomez-Navarro C, Weitz RT, Bittner AM, Matteo S, Mews A, Burghard M, Kern K. Electronic transport properties of individual chemically reduced graphene oxide sheets. Nano Lett. 2007; 7:3499–3503. [PubMed: 17944526]
36. Wang H, Wang L, Qu C, Su Y, Yu S, Zheng W, Liu Y. Photovoltaic properties of graphene oxide sheets beaded with ZnO nanoparticles. J Solid State Chem. 2011; 184:881–887.
37. Chen Y, Hu Z, Chang Y, Wang H, Zhang Z, Yang Y, Wu H. Zinc oxide/reduced graphene oxide composites and electrochemical capacitance enhanced by homogeneous incorporation of reduced graphene oxide sheets in Zinc oxide matrix. J Phys Chem C. 2011; 115:2563–2571.
38. Jiang G, Lin Z, Chen C, Zhu L, Chang Q, Wang N, Wei W, Tang H. TiO_2 nanoparticles assembled on graphene oxide nanosheets with high photocatalytic activity for removal of pollutants. Carbon. 2011; 49:2693–2701.
39. Wang G, Yang J, Park J, Gou X, Wang B, Liu H, Yao J. Facile synthesis and characterization of graphene nanosheets. J Phys Chem C. 2008; 112:8192–8195.
40. Xu C, Wang X, Zhu JW, Yang XJ, Lu L. Deposition of Co_3O_4 nanoparticles onto exfoliated graphite oxide sheets. J Mater Chem. 2008; 18:5625–5629.
41. Stankovich S, Dikin D, Piner RD, Kohlhaas KA, Kleinhammes A, Jia Y, Wu Y, Nguyen ST, Ruoff RS. Synthesis of graphene-based nanosheets via chemical reduction of exfoliated graphite oxide. Carbon. 2007; 45:1558–1565.
42. Wang J, Tsuzuki T, Tang B, Hou X, Sun L, Wang X. Reduced graphene oxide/ZnO composite: reusable adsorbent for pollutant management. ACS Appl Mater Interfaces. 2012; 4:3084–3090. [PubMed: 22676310]
43. Zhu C, Guo S, Wang P, Xing L, Fang Y, Zhai Y, Dong S. One-pot, water-phase approach to high-quality graphene/TiO_2 composite nanosheets. Chem Commun. 2010; 46:7148–7150.
44. Wan Q, Wang TH, Zhao JC. Enhanced photocatalytic activity of ZnO nanotetrapods. Appl Phys Lett. 2005; 87:83105/1–3.

Research Highlights

- Development of novel method for synthesis of graphene-ZnO catalyst.
- Prepared photocatalysts possessed great adsorptivity of rhodamine B.
- Complete degradation of rhodamine B occured in presence of natural sunlight.
- Sensitization of graphene-ZnO catalyst with CoPC has improved its photoresponsivity.

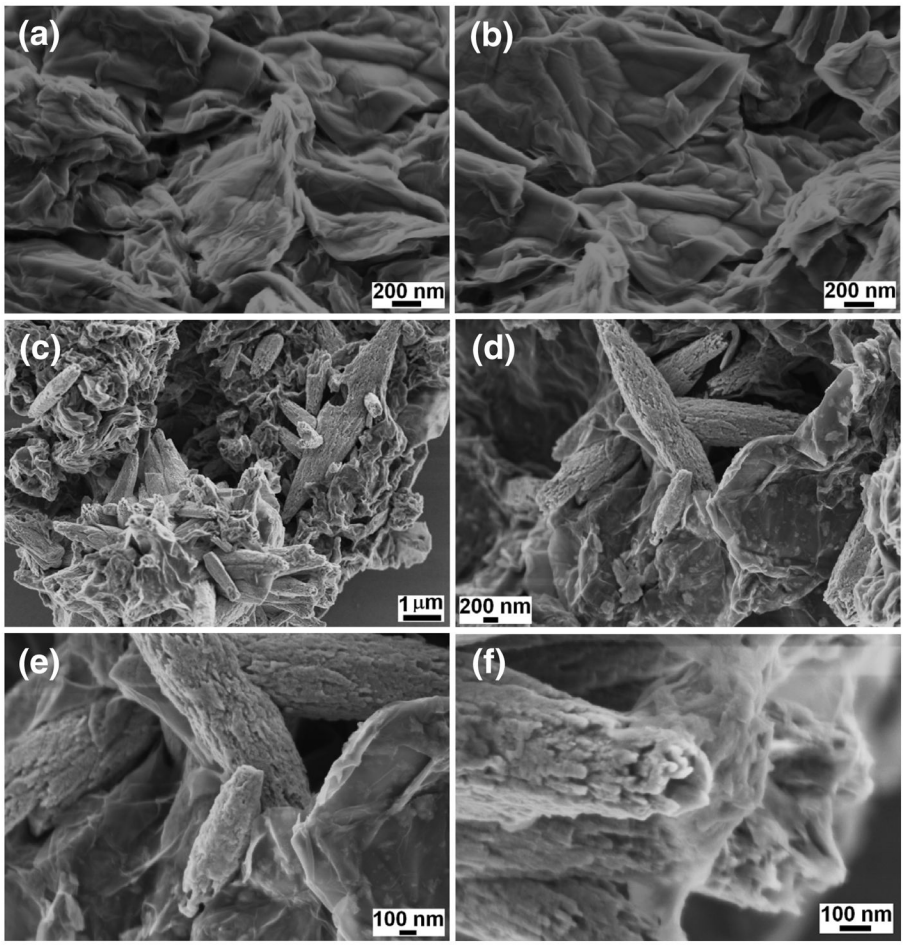

Fig. 1.
SEM images of (a,b) GO and (c–f) GR-ZnO catalyst.

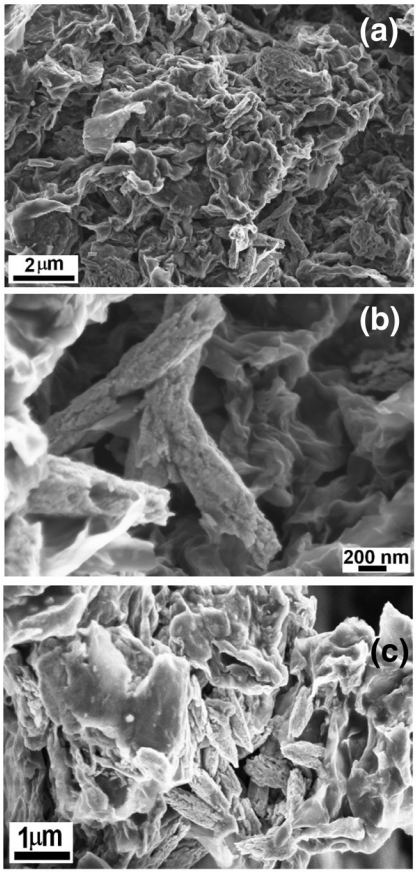

Fig. 2.
SEM images of GR-ZnO-CoPC catalyst.

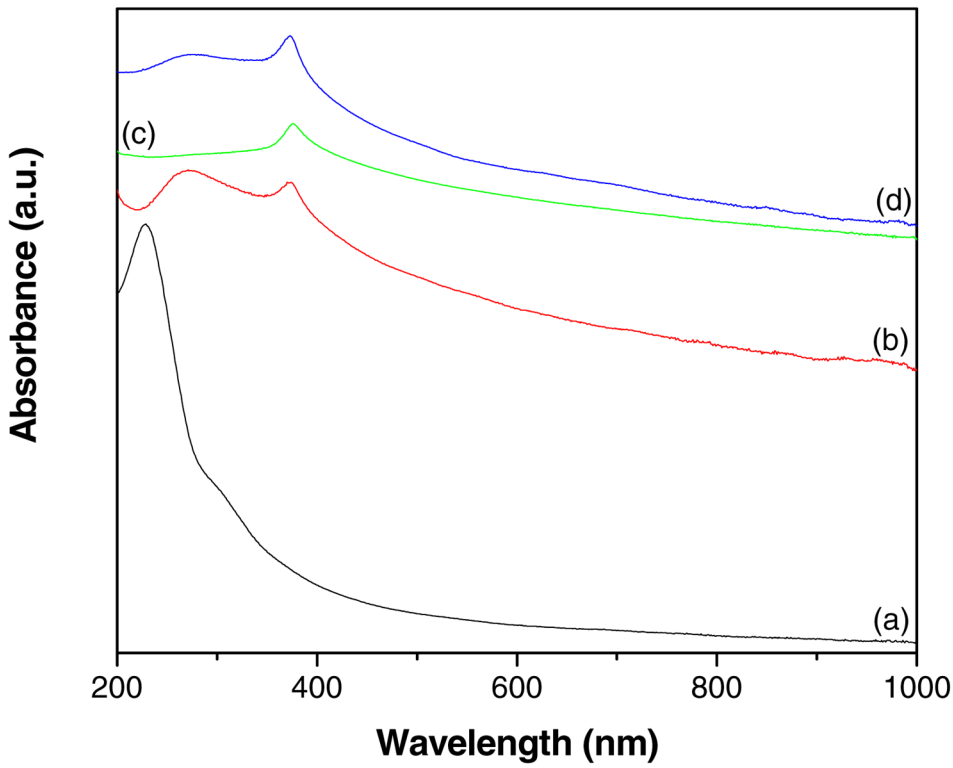

Fig. 3.

UV-vis absorption spectra of (a) GO, (b) GR-ZnO catalyst, (c) ZnO particles and (d) GR-ZnO-CoPC catalyst.

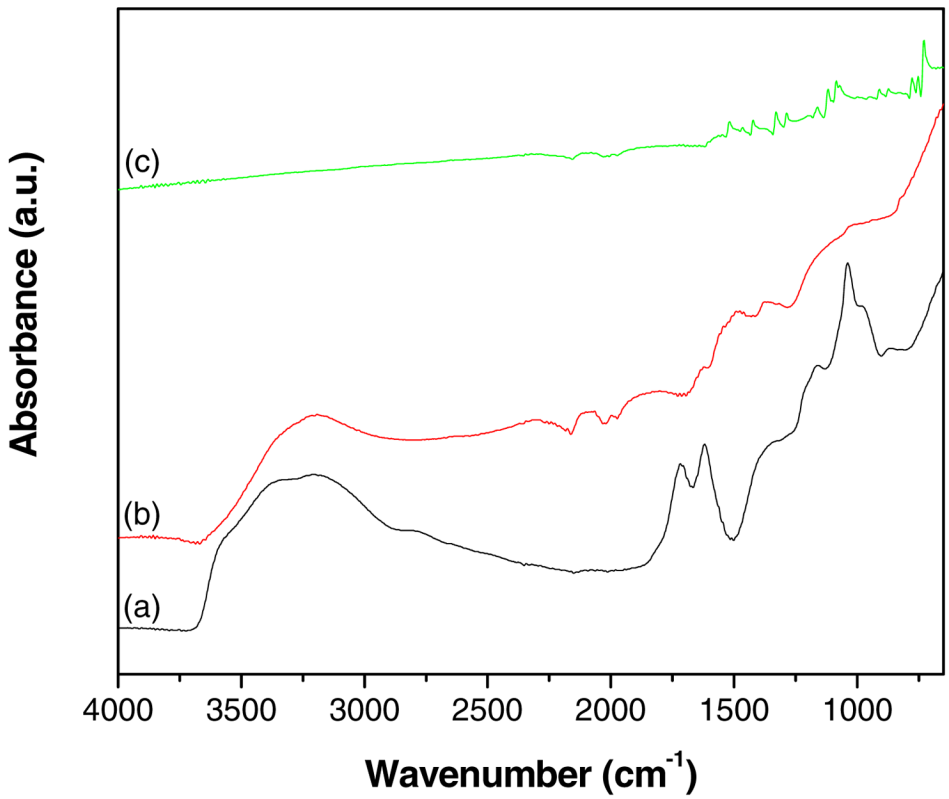

Fig. 4.
ATR-IR spectra of (a) GO, (b) GR-ZnO catalyst and (c) GR-ZnO-CoPC catalyst.

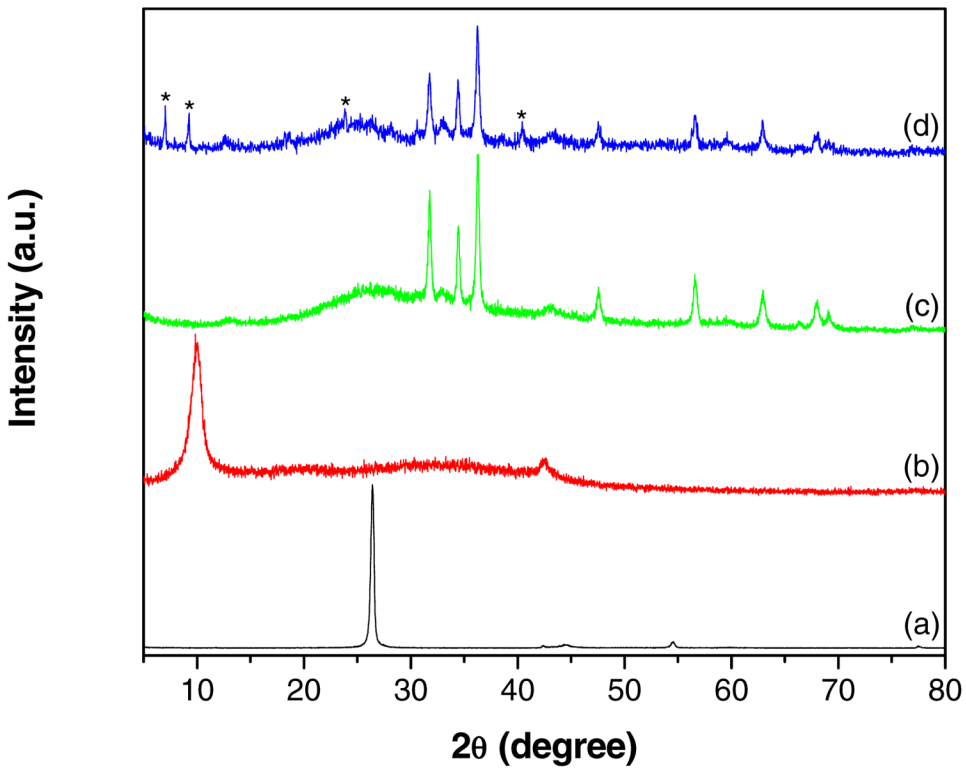

Fig. 5.

XRD patterns of (a) graphite, (b) GO, (c) GR-ZnO catalyst and (d) GR-ZnO-CoPC catalyst (the peaks corresponding to CoPC are indicated with *).

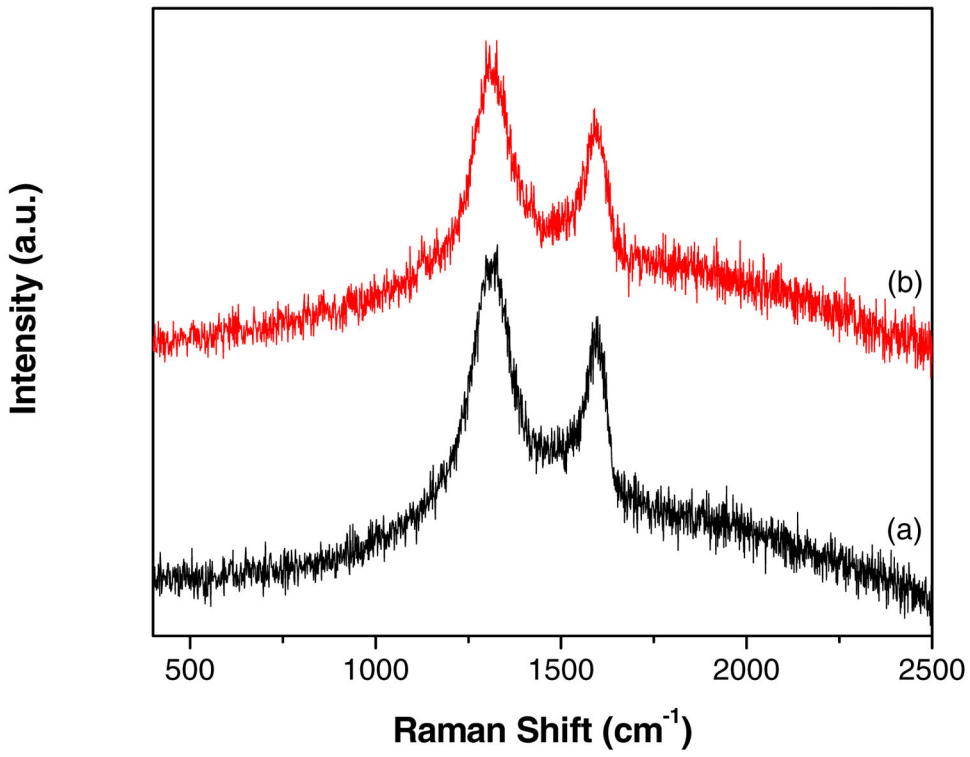

Fig. 6.
Raman spectra of (a) GO and (b) GR-ZnO catalyst.

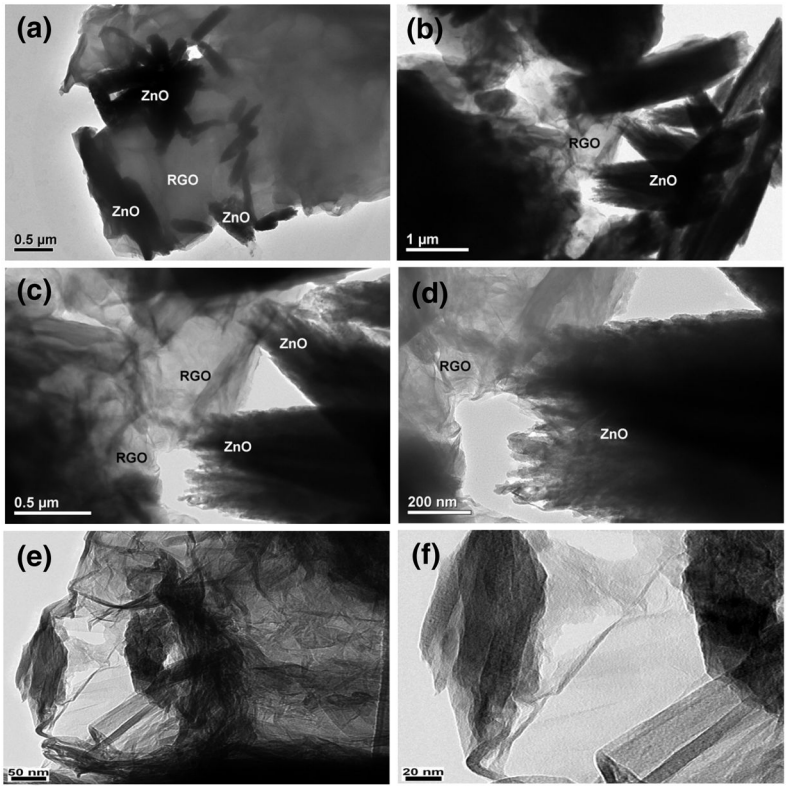

Fig. 7.
TEM images of (a–d) GR-ZnO catalyst and (e,f) GR-ZnO-CoPC catalyst.

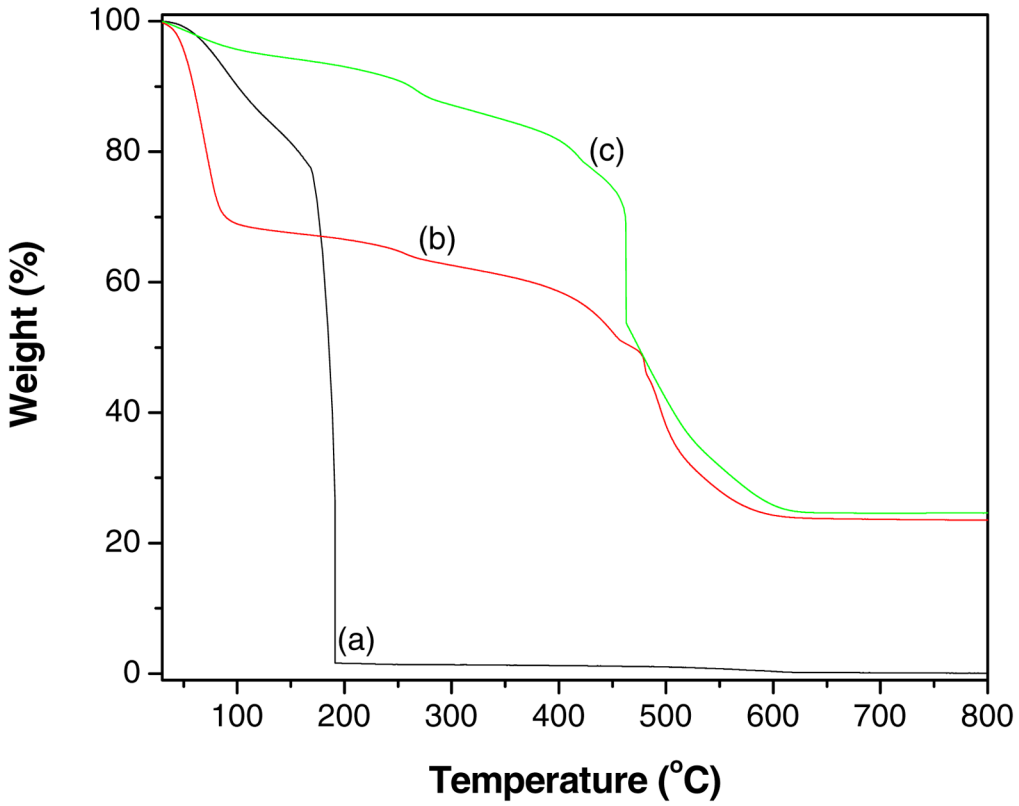

Fig. 8.
TGA profiles of (a) GO, (b) GR-ZnO catalyst and (c) GR-ZnO-CoPC catalyst.

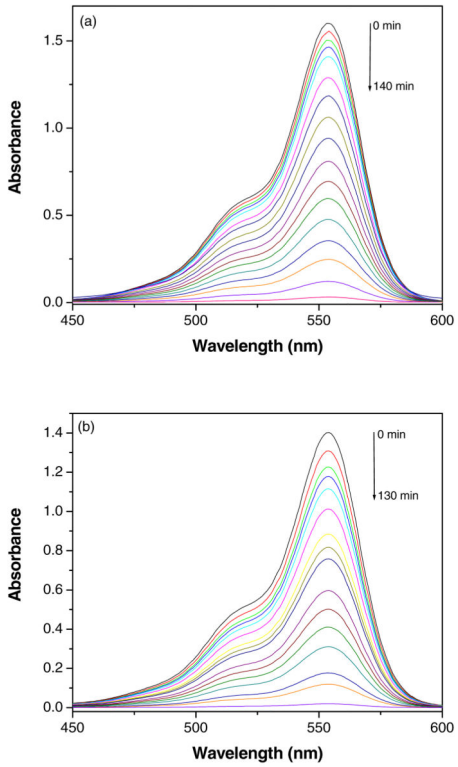

Fig. 9.

Decrease in the UV-vis absorption band of Rh B in presence of (a) GR-ZnO catalyst and (b) GR-ZnO-CoPC catalyst at different time of exposure to sunlight.

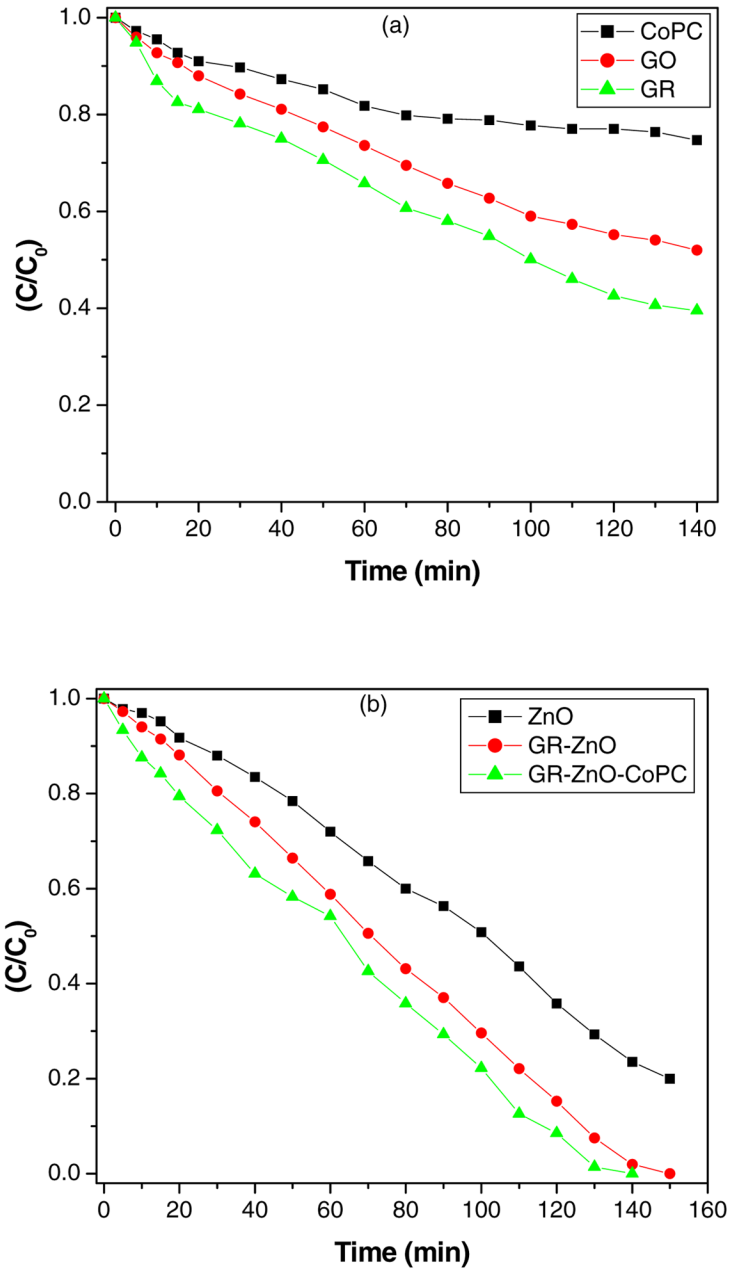

Fig. 10.

Profie of photocatalytic degradation of RhB in presence of (a) CoPC, GO and GR, and (b) ZnO, GR-ZnO catalyst and GR-ZnO-CoPC catalyst.

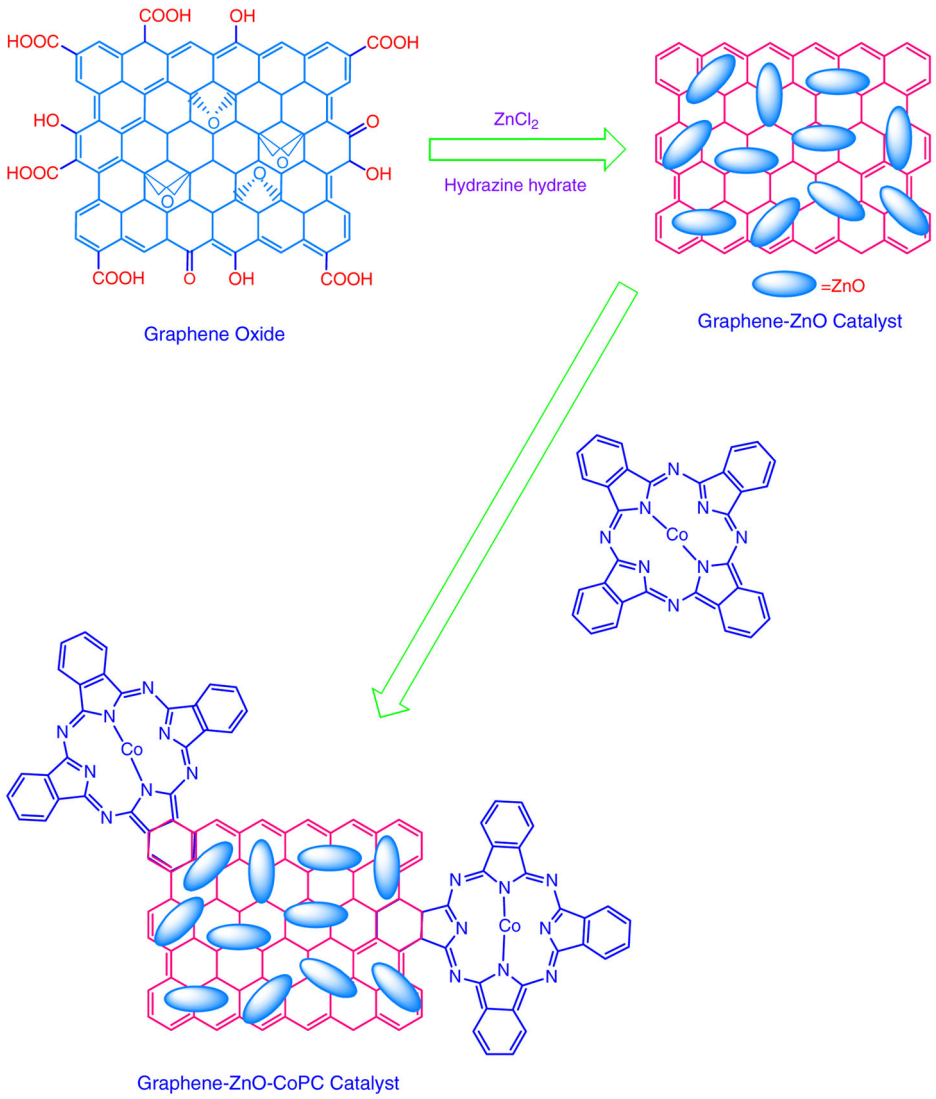

Scheme I.
Preparation of GR-ZnO catalyst and its sensitization with CoPC.